JOURNAL OF AIRCRAFT
Vol. 37, No. 4, July–August 2000

Aerodynamic Design of a Flying Wing Using Response Surface Methodology

Natasha E. Sevant,* Malcolm I. G. Bloor,† and Michael J. Wilson‡
University of Leeds, Leeds, England LS2 9JT, United Kingdom

The design of a subsonic flying wing with maximized lift is considered. A novel method of surface generation, known as the partial differential equation (PDE) method, is used to parameterize the flying wing. Because this method is able to parameterize complex geometries in terms of a small number of shape parameters, the computational costs that are normally associated with optimal aerodynamic design are dramatically reduced. The lift data, which are estimated using a low-order potential flow panel method, are subject to numerical noise and yield, therefore, a design space that contains many spurious noise-induced local maxima. Standard methods of local optimization are severely hampered by this noise and may converge prematurely in nonoptimal plateau regions where the variation of the lift is small relative to that of the noise. To combat this inefficiency, techniques from response surface methodology (RSM) are used to construct smooth analytic approximations of the noisy lift data, which can be optimized successfully. This combination of the PDE method and RSM results in a design approach that is both efficient and robust. Three flying-wing design problems are investigated, and the results are presented.

Nomenclature

a	= smoothing parameter
C	= reference length
C_L, C_l	= total and section coefficients of lift
c	= aerofoil camber
c_r, c_t	= root and tip aerofoil chord lengths
$\mathrm{d}S_B$, $\mathrm{d}S_W$	= surface elements on wing and wake
$f(\boldsymbol{X}, \beta)$	= regression equation
K_P	= parameter depending on position of P relative to S_B
L, L'	= total lift and lift per unit span
M	= number of regression parameters
N	= number of response evaluations
n	= order of Fourier mode or number of independent design variables
$\boldsymbol{n}$	= unit normal vector
n_0	= number of center points in central composite design
P	= point
r	= distance between P and either $\mathrm{d}S_B$ or $\mathrm{d}S_W$
S	= plan-area of wing or reference area
S_B, S_W	= surfaces of the wing and the wake
s_r, s_t	= derivative boundary condition scaling parameters
t_1, t_2	= Fourier coefficients of aerofoil thickness distribution
u, v	= parametric surface coordinates
V_∞	= far-field reference speed
$\boldsymbol{X} = (X_1, \ldots, X_n)$	= independent design variables
$\boldsymbol{x} = (x, y, z)$	= Cartesian coordinates
x_c, y_c, z_c	= x, y, and z coordinates of cambered template aerofoil
x_s, y_s, z_s	= x, y, and z coordinates of symmetric template aerofoil
x_t, y_t	= axial and spanwise positions of wing tip
$\boldsymbol{x}_0$, $\boldsymbol{x}_n^c$, $\boldsymbol{x}_n^s$	= functions of the parametric coordinate u
y	= actual response values
y_k	= observed response values
$\hat{y}_k$	= predicted response values
α	= geometric twist of tip aerofoil or central composite design parameter
$\beta = \{\beta_0, \beta_i, \beta_{ij}\}$	= regression parameters
$\partial\Omega$	= boundary of parameter domain Ω
η	= expected or mean response
μ	= wing doublet strength distribution
μ_B, μ_W	= wing and wake doublet strengths
μ_P	= doublet strength at point P
ρ	= density
σ	= wing source strength distribution
σ_B	= wing source strength
Φ	= velocity potential
Φ_P	= velocity potential at point P
ϕ_∞	= onset velocity potential
$\phi_{\infty P}$	= onset velocity potential at point P
Ω	= two-dimensional parameter domain

Received 27 May 1998; revision received 15 January 2000; accepted for publication 20 March 2000.

*Research Fellow, Department of Applied Mathematics. Member AIAA.
†Professor, Department of Applied Mathematics. Member AIAA.
‡Reader, Department of Applied Mathematics. Member AIAA.

Introduction

DESPITE being unconventional, flying wings—which, as their name suggests, consist of a solitary wing—are considered to be a viable aircraft configuration. They were first conceived by Jack Northrop in the late 1920s,[1] and in the aftermath of World War II, the U.S. Air Force awarded a contract to Northrop's company to build a number of flying-wing bombers. Although this contract was shortly cancelled, today there is a revival of interest in flying wings for use as stealth aircraft (such as the Northrop B-2 bomber and the British HALO bomber) and as advanced, fuel-efficient cargo planes.[2,3] In this paper the aerodynamic design of a simplified flying wing with maximized subsonic lift is considered. It must be made clear however that, because sufficient lift is only one of the many factors to be considered when designing real aircraft, the aim of this paper is to illustrate the application of two innovative techniques to aerodynamic design rather than to design a completely realistic flying wing.

Direct numerical optimization is an approach to aerodynamic design that involves coupling an aerodynamic analysis method with a scheme for numerical minimization where the aim is the direct attainment of certain aerodynamic goals, such as maximum lift and/or minimum drag. Unfortunately, however, direct numerical optimization is computationally expensive; the principle source of this expense can be attributed to the repetitive executions of costly aerodynamic analysis methods. Labrujère and Slooff[4] identify three major

factors that warrant further consideration in attempts to make direct numerical optimization more feasible. These factors are the following: the choice of an objective function—subject to the capabilities of available analysis codes—that adheres to the design requirements; a reduction in the number of design variables used to describe the geometry of the aircraft; and the choice of an efficient and robust optimization algorithm.

The second of these factors, a reduction in the number of design variables, has been considered in many applications of direct numerical optimization. For example, Hicks and Henne[5] use a successful two-dimensional aerofoil design technique (which uses a linear combination of analytic shape perturbation functions) in the design of a three-dimensional transonic wing. However, they remark that the development of a more flexible wing parameterization is necessary. A similar more sophisticated two-dimensional concept was introduced by Aidala et al.,[6] which uses the aerofoil section ordinate perturbation solutions (known as aerofunction shapes) of inverse design problems. Although this technique allows a more effective choice of designer variables (because their aerodynamic influences are prescribed), the optimizer will be limited to a restricted range of anticipated shapes. More recently, Hutchison et al.[7] have developed a wing parameterization technique in which the number of parameters are reduced by relating the aerofoil sections to the wing planform according to standard aerodynamic practice. Again, however, this method of parameterization may limit the optimizer to a restricted range of anticipated shapes.

In this paper the flying wing is parameterized by using an alternative technique known as the partial differential equation (PDE) method. This is a novel method of surface generation that is able to parameterize complex surfaces efficiently without severely limiting the range of available shapes. This low level of parameterization and versatility in the range of available shapes enables direct numerical optimization to be fully exploited without incurring large computational costs.

The third factor identified by Labrujère and Slooff[4] for reducing computational expense is the use of an efficient and robust method of optimization. In this paper the subsonic lift data, which are calculated using a low-order potential flow panel method, contain noise. The objective function (i.e., the lift) displays, therefore, a jagged variation with the wing design parameters. This noise can cause a standard method of optimization to be inefficient and, also, to converge prematurely to a noise-induced maximum (particularly if the variation of the objective function is small compared with that of the noise). To combat these problems, techniques from response surface methodology are used to construct smooth analytic approximations (known as response surfaces) of the noisy objective function, which can then be optimized using any standard method of optimization.

PDE Method

The PDE method is an innovative method of surface generation, which was devised by Bloor and Wilson.[8] This method has been used to design many surfaces of practical significance, such as generic aircraft geometries,[9,10] a wing-body combination,[11] and marine propellers.[12]

In the PDE method a surface is given by a parametric function $\boldsymbol{x}(u, v)$ defined over a domain Ω in two-dimensional (u, v) parameter space. Such a function is obtained as the solution of an elliptic PDE subject to boundary conditions specified around the edge $\partial\Omega$ of the domain Ω. Much of the previous work has been based upon the following fourth-order elliptic PDE:

$$\left(\frac{\partial^2}{\partial u^2} + a^2\frac{\partial^2}{\partial v^2}\right)^2 \boldsymbol{x} = 0 \tag{1}$$

where a (which controls the relative scaling between the u and v parametric directions) is known as the smoothing parameter and the boundary conditions usually specify how $\boldsymbol{x}$ and its normal derivative $\partial\boldsymbol{x}/\partial n$ (which controls the direction and speed of departure of the surface from its boundaries) vary along $\partial\Omega$.

Many surfaces can be represented by a looped surface patch bounded by two closed curves or can be constructed from a collection of such patches. For surfaces such as these, it is convenient to choose one of the parameters, u say, to vary as the surface sweeps from one boundary curve to the other, whereas the other parameter v varies around the patch. Choosing the v interval to be $[0, 2\pi]$ yields a parametric function $\boldsymbol{x}(u, v)$ with a period of 2π in v, which can thus be expressed in terms of a Fourier series expansion, as follows:

$$\boldsymbol{x}(u, v) = \boldsymbol{x}_0(u) + \sum_{n=1}^{\infty} \boldsymbol{x}_n^c(u)\cos nv + \sum_{n=1}^{\infty} \boldsymbol{x}_n^s(u)\sin nv \tag{2}$$

where the components of the vectors $\boldsymbol{x}_0$, $\boldsymbol{x}_n^c$, and $\boldsymbol{x}_n^s$ are functions of u. Substituting this Fourier series expansion into Eq. (1) yields an uncoupled series of identical linear homogeneous ordinary differential equations for the functions $\boldsymbol{x}_0$, $\boldsymbol{x}_n^c(u)$, and $\boldsymbol{x}_n^s(u)$—each with a solution that is dependent upon the relevant Fourier mode of the boundary conditions. For more general boundary conditions, which cannot be expressed exactly as finite Fourier series, Bloor and Wilson have developed a rapid approximate method of solution.[13]

Wing Geometry

A simple cambered template aerofoil, of unit chord length, can be represented by the following Fourier series:

$$[x_c(v),\ x_c(v),\ x_c(v)] = \left[\tfrac{1}{2}\cos v,\ 0,\ t_1 \sin v + t_2 \sin 2v + (c/2)(1 - \cos 2v)\right] \tag{3}$$

where v varies in the range $0 \le v \le 2\pi$. The Fourier coefficients t_1 and t_2 define the thickness distribution of the aerofoil, whereas the parameter c controls the amount of camber. Choosing this camber to be zero yields a symmetric template aerofoil, for which the camber-denoting subscript c is replaced by s to denote symmetry.

The positional boundary conditions required to generate a twisted flying wing with a cambered root aerofoil and a symmetric tip aerofoil can be formed by scaling, translating, and rotating these template aerofoils, as follows:

$$\boldsymbol{x}(0, v) = c_r \begin{pmatrix} x_c(u) \\ 0 \\ z_c(u) \end{pmatrix}$$

$$\boldsymbol{x}(1, v) = \begin{pmatrix} x_t \\ y_t \\ 0 \end{pmatrix} + c_t \begin{pmatrix} x_s(u)\cos\alpha + z_s(u)\sin\alpha \\ 0 \\ z_s(u)\cos\alpha - x_s(u)\sin\alpha \end{pmatrix} \tag{4a}$$

where the parameter u is taken to be zero at the wing root and unity at the wing tip and y_t is the wing semispan.

The derivative boundary conditions are taken to be

$$\boldsymbol{x}_u(0, v) = \begin{pmatrix} 0 \\ s_r \\ 0 \end{pmatrix}$$

$$\boldsymbol{x}_u(1, v) = -s_t \begin{pmatrix} x_s(u)\cos\alpha + z_s(u)\sin\alpha \\ 0 \\ z_s(u)\cos\alpha - x_s(u)\sin\alpha \end{pmatrix} \tag{4b}$$

where the magnitudes of parameters s_r and s_t control the speed with which the surface departs from its boundary curves and their sign determines the direction of departure. These derivative boundary conditions are such that the flying wing is the tangent plane continuous both across its plane of symmetry $y = 0$ and with the plane $y = y_t$ defined by its tip aerofoil.

The wing surface can now be found by the solution of Eq. (1) subject to the boundary conditions (4a) and (4b). Figure 1 illustrates a baseline flying wing that has the following parameter values: $t_1 = 0.05$, $t_2 = -0.02$, $c = 0$, $c_r = 5.0$, $c_t = 1.0$, $x_t = 0.0$, $y_t = 10.0$,

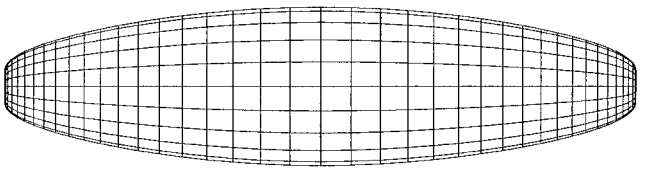

Fig. 1 Baseline flying wing.

$\alpha = 0$ deg, $s_r = 20.0$, $s_t = 5.0$, and $a = 2.1183$ [where the smoothing parameter a was determined using a bisection search such that the plan area of the semispan wing, as given by Eq. (5), is equal to 40.0].

In the wing design problems to be considered, the sweep parameter x_t, the derivative boundary condition parameters s_r and s_t, and the smoothing parameter a of the surface-generating PDE are permitted to vary. Certain bound constraints need to be imposed on these parameters in order to maintain sensible geometries. For example, to ensure the intended direction of departure of the wing from the root and tip boundary aerofoils, both the parameters s_r and s_t must be greater than or equal to zero. It is also required that the solution $y(u)$ (which is a function of only u because its boundary conditions are independent of v) of Eq. (1) increases monotonically over the range [0, 1]. From Eq. (4b) $y(u)$ has a stationary point at $u = 1$, and for the function to be monotonically increasing over the range [0, 1], this stationary point must either be a maximum turning point or a point of inflection. Thus, we require that $y_{uu}(1) \geq 0$, which reduces to $s_r \leq 3y_t$. Finally, to avoid numerical difficulties, the smoothing parameter a is constrained to be greater than or equal to unity.

The semispan wing is constrained to have a fixed plan area S, which, for $\alpha = 0$ deg, can be evaluated directly (and, for small α, can be approximated) using the formula

$$S = \int_0^1 y_u(u) \int_\pi^0 x_v(u, v)\, \mathrm{d}v\, \mathrm{d}u \tag{5}$$

Subsonic Analysis

A low-order potential-flow panel method, known as PMARC,[14] is used to estimate the lift of the flying wing. Panel methods are based on the assumption that, for high Reynolds number and attached flow conditions, the regions of the flowfield dominated by viscous and rotational effects are confined to thin boundary layers and wakes. The remainder of the flowfield is assumed to be inviscid, irrotational, and also incompressible. Thus, a velocity potential Φ can be defined, and the incompressible continuity equation reduces to Laplace's equation $\nabla^2\Phi = 0$. The solution of this equation yields an integral equation for the velocity potential Φ_P, at any point P, expressed in terms of an unknown distribution of sources σ and doublets μ across the surface of the wing S_B and an unknown distribution of doublets μ_W across the surface of the wake S_W, as follows:

$$\Phi_P = \frac{1}{4\pi}\left[\iint_{S_B - P} \mu\, \boldsymbol{n} \cdot \nabla\left(\frac{1}{r}\right) \mathrm{d}S_B + K_P \mu_P + \iint_{S_B} \left(\frac{\sigma}{r}\right) \mathrm{d}S_B + \iint_{S_W} \mu_W \boldsymbol{n} \cdot \nabla\left(\frac{1}{r}\right) \mathrm{d}S_W \right] + \phi_{\infty_P} \tag{6}$$

where the subscript $S_B - P$ signifies that the point P is excluded from the first surface integral and the value of the parameter K_P depends on where P lies with respect to the surface.[14]

Equation (6) must satisfy the Neumann boundary condition, which states that the velocity component normal to the surface of the wing S_B is zero. Also, because potential flow is irrotational, a physically based condition must be introduced to fix the amount of circulation and, equivalently, the amount of lift generated by the wing. In PMARC the Kutta condition, which ensures that the velocity at a wing's trailing edge is finite, is used to fix the amount of lift generated by the wing.

Even subject to the Neumann boundary and Kutta conditions, an infinite number of source and doublet distributions will satisfy Laplace's equation, each of which yields the same external flowfield but different fictitious flowfields within the interior of the wing. To obtain a unique solution, PMARC sets the fictitious internal velocity potential equal to the onset velocity potential ϕ_∞, a condition which is known as the internal Dirichlet boundary condition. The source distribution σ, which is the jump in the normal velocity component on the surface of the wing S_B, can thus be determined using the external Neumann and internal Dirichlet boundary conditions. Substituting this source distribution into Eq. (6) when the point P lies on the inner surface of the wing yields an integral equation to be solved for the unknown doublet distributions μ and μ_W.

To obtain the unknown doublet distribution, the surfaces of the wing and its wake are discretized into a number of quadrilateral panels, upon each of which (because PMARC is a low-order panel method) constant source and doublet strengths are assumed. The PDE-generated wing considered here is easily discretized by uniformly subdividing the (u, v) coordinate domain which, as a result of the parameterization of the boundary conditions, conveniently yields a greater density of panels in the regions of large pressure variations (i.e., at the leading and trailing edges and also at the wing tip—see Fig. 1).

The internal Dirichlet boundary condition is satisfied at control points placed at the center of each of the wing's surface panels. This yields a set of linear simultaneous equations, which can be solved for the unknown wing doublet strengths. The wake doublet strengths are determined using the Kutta condition, which implies that the circulation at the wing's trailing edge must be zero and therefore that the doublet strengths of the first row of wake panels should cancel the combined doublet strengths of the two rows of wing panels that form the trailing edge of the wing. Although PMARC has the capability to time step wakes to a converged solution, in the present application computational expense is reduced by shedding the wake doublet strengths down each streamwise column on a prescribed wake surface that is carried 20 chord lengths downstream (as recommended in Ref. 15).

Substituting the doublet and source strengths back into the discretized form of Eq. (6) yields the velocity potential at the control point of each wing panel. The velocity components are then given by the gradient of the velocity potential from which the resultant speeds can be calculated. For steady flow the pressure coefficients of each panel can then be calculated using Bernoulli's equation, and, thus, the resultant force contributions from each panel can be evaluated. These force contributions can be summed up panel by panel, to give the resultant aerodynamic force on the body. The lift L is the component of this resultant force perpendicular to the freestream direction, and the section and total lift coefficients C_l and C_L are defined by

$$C_l \equiv L' \Big/ \tfrac{1}{2}\rho V_\infty^2 C \qquad C_L \equiv L \Big/ \tfrac{1}{2}\rho V_\infty^2 S \tag{7}$$

Optimization and Constraints

The method of numerical minimization used in this paper is a quasi Newton method. Such methods use gradient information to search in descent directions for the minimum of an objective function. The direction of each line search is determined by minimizing the second-order Taylor-series expansion of the objective function. This involves evaluating or approximating both the gradient vector and the inverse Hessian matrix of the objective function. Quasi Newton methods build up an approximation to the inverse Hessian matrix, and the various different methods correspond to different ways of approximating this matrix. The particular method used in this paper is the Broyden–Fletcher–Goldfarb–Shanno (BFGS) method.[16]

The flying-wing design problem is subject to two types of constraints: linear inequality constraints (the parameter bounds) and an equality constraint (the fixed plan area). The parameter bound inequality constraints are satisfied using an active set method.[17] If, during a line search, a parameter exceeds one of its bounds, the search is backtracked to satisfy this bound constraint exactly. If this point is accepted as the solution of the line search, this parameter is then set equal to the value of its active bound and thus eliminated from the search. At the end of the optimization, each active bound

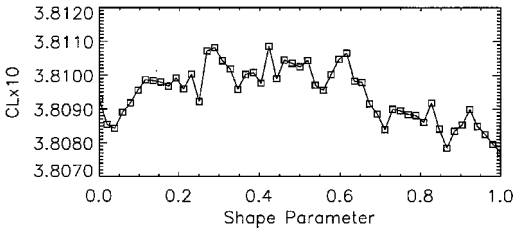

Fig. 2 Variation of the coefficient of lift along a feasible slice of the design space.

constraint must be checked to ensure that it has remained active. If one (or more) of the active bound constraints is invalid (i.e., if a feasible perturbation yields a decrease in the objective function), then the parameter corresponding to the invalid bound constraint (or the one which is the most invalid) is returned to the problem and the optimization restarted. This process continues until all active constraints are valid.

The plan area equality constraint is satisfied using a sequential penalty function method. Penalty function methods satisfy constraints by penalizing constraint violations. This entails adding a smoothly rising penalty term to the objective function when constraints are violated. For a strong penalty function this results in a steep-sided valley, which is well known for being difficult to minimize because the line searches tend to tack along the valley floor. The penalty function is therefore applied sequentially, starting with a weak penalty and then gradually increasing its strength. The solution of each penalty function provides a new starting point, which should be nearby to the solution of the next penalty function.

Discussion of Noise

Initially, the flying-wing design problem was attempted by directly coupling the BFGS method of optimization with the panel method PMARC and approximating the gradient vector of the objective function (i.e., the lift) using finite differences. However, unsatisfactory results were obtained. This prompted an investigation into the design space, and it was discovered that the lift data obtained using PMARC are noisy. This noise results in a jagged objective function that contains many spurious noise-induced local maxima. It was hoped that finite difference intervals that were large enough to span the scale of the noise would enable more successful results. Unfortunately, however, the results were still unsatisfactory.

Figure 2 illustrates the variation of the coefficient of lift along a feasible slice of the design space. The optimization process was becoming trapped in plateau regions of the feasible design space where the variation of the lift is small relative to the amplitude of the noise. In such regions, even with the choice of relatively large finite difference step lengths, the finite difference approximations yield erroneous search directions that handicap the progress of the optimizer and cause it to converge prematurely to spurious noise-induced maxima.

Response Surface Methodology

Response surface methodology (RSM) is a collection of mathematical and statistical techniques for solving problems in which the goal is to optimize the response y of a system or process that is influenced by n independent variables $\boldsymbol{X} = (X_1, X_2, \ldots, X_n)$ and is subject to observational errors.[18]

A response surface is a smooth analytic function that represents the true functional relationship between the expected or mean value η of the response and its n independent variables $\boldsymbol{X} = (X_1, X_2, \ldots, X_n)$. Usually, because this relationship is not known, the assumption is made that it can be approximated locally by a second-order polynomial of the form

$$f(\boldsymbol{X}, \boldsymbol{\beta}) = \beta_0 + \sum_{i=1}^{n} \beta_i X_i + \sum_{i=1}^{n} \sum_{j=1}^{i} \beta_{ij} X_i X_j \qquad (8)$$

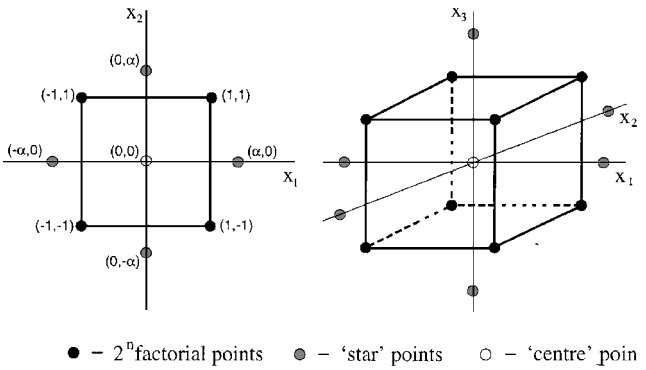

Fig. 3 Central composite designs for two and three design variables.

where β_0, β_i, and β_{ij} are unknown polynomial coefficients or regression parameters and Eq. (8) is referred to as a regression equation.

Estimates of the regression coefficients β_0, β_i, and β_{ij} can be made by fitting Eq. (8) to the response surface values observed at a set of data points. Equation (8) has $(n + 1)(n + 2)/2$ unknown regression parameters, and in order to estimate these, at least an equal number of data points is required. The quality of the fitted response surface increases as the number of data points increases. Also, the condition number, i.e., the ratio of the highest eigenvalue to the lowest, of the least-squares matrix decreases as the number of data points increase (as is desirable to avoid near-singular matrices). However, to maintain low computational costs, the total number of response evaluations should be kept reasonably low.

A further consideration in the choice of data points is their distribution: a poor distribution can have a profound effect upon the fidelity of the fitted response surface. To choose suitable distributions of data points, RSM uses methods from the statistical design of experiments.[18]

Classes of designed experiments, which were devised specifically for fitting second-order response surfaces, are the central composite designs. These designs consist of a 2^n-factorial design augmented by $2n$ axial or star points and n_0 center points. A (full) factorial design is one that uses every possible combination of the chosen levels (values) of each factor (independent variable). If each of the independent variables are scaled such that the 2^n factorial or cube points can be coded by $(\pm 1, \pm 1, \ldots, \pm 1)$, then each of the $2n$ star points lie at a coded distance α from the center $(0, 0, \ldots, 0)$ of the factorial design. Therefore, the response is evaluated at five levels of each variable, coded by $(-\alpha, -1, 0, 1, \alpha)$, as illustrated in Fig. 3, which shows the central composite designs for two and three design variables. The number n_0 of center points can be used to control various properties of the central composite design; in this paper n_0 is set to unity.

Because the purpose of RSM is optimization and the location of that optimum is not known prior to performing the experiment, it is sensible to use an experimental design that provides equal precision in all directions. Such an experimental design is said to be rotatable and yields a predicted response whose variance, at a point $\boldsymbol{X}$, is a function of only the distance of that point from the design's center point and not the direction. The central composite designs used in this work can be made rotatable by selecting the value of α to be $(2^n)^{1/4}$.

Estimates of the regression parameters $\boldsymbol{\beta}$ are obtained by performing a least-squares fit of the regression Eq. (8) to the response values obtained at each of the data points defined by the central composite design. The least-squares problem is solved using singular value decomposition.[16]

It is important to check whether the tentatively assumed response surface model is an adequate approximation of the data. A measure of the modeling capabilities of the response surface is given by the residual mean square (RMS):

$$\text{RMS} = \frac{\sum_{k=1}^{N} (y_k - \hat{y}_k)^2}{N - M} \qquad (9)$$

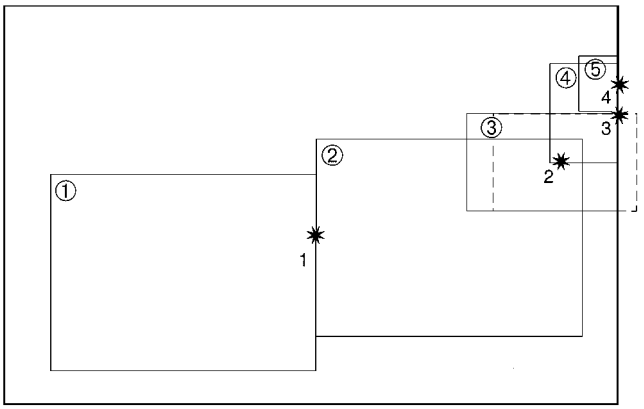

Fig. 4 Example sequence of search subregions.

where the residual is defined as the difference between the response values y_k and the corresponding values predicted by the fitted response surface $\hat{y}_k$. The terms M and N are the number of unknown parameters and the number of response evaluations [which are equal to $(n + 1)(n + 2)/2$ and $2^n + 2n + 1$ for the second-order polynomial and the central composite design, respectively]. The RMS contains two sources of variation: a contribution caused by the experimental (or numerical) error, known as the pure error sum of squares, which makes the values of y deviate from the true or expected response, and a contribution caused by the failure of the model to represent the correct form of the response surface variation, known as the lack of fit sum of squares. Because the response (i.e., lift) in this paper is evaluated deterministically and the numerical error for each evaluation will be the same for each replication, an estimate of the variance caused by the error is not possible. Nevertheless, a small value of the RMS with respect to the total variation of the response values obtained using the central composite design can be considered to indicate an adequate fit.

Optimization Using Sequential Response Surfaces

A second-order response surface is unlikely to provide an adequate approximation of the objective function over a large region of design space. Therefore, a sequential approach is used in which smaller and smaller subregions of the design space are approximated such that convergence to an optimal design is achieved. To perform this sequential response surface optimization process, a strategy similar to those of Refs. 19 and 20 is used. The size and location of each subregion depends on where the optimal point of the previous subregion lies with respect to the boundaries of both that subregion and the entire search region. Figure 4 illustrates a contrived example of a sequence of search subregions for a two-dimensional problem. In this figure the thin and thick lines define the parameter bound constraints of the search subregions and the entire search region, respectively, whereas the increasing numbers in the top left-hand corner of each rectangle correspond to each subsequent search subregion and the numbered stars represent the optimal points of those subregions.

If the optimal point of a subregion has any active parameter bound constraints (that are not coincident with those of the entire region), as for the optimal point of subregion 1, then the subregion lies in a nonoptimal region of the parameter space. The subsequent subregion is obtained by projecting the previous subregion, without a reduction in size, in the direction indicated by the optimal point of the previous region such that it becomes adjacent to the previous subregion, as for subregion 2. If, however, the optimal point lies in the interior of the previous subregion, i.e., all of the subregion-bound constraints of the optimal point are inactive, as for the optimal point of region 2, then that point is regarded as an approximation of the true optimal point, and the next subregion is centered about that optimal point and also reduced in order to converge toward that optimal point, as for subregion 3. In the Fig. 4, scenario this has resulted in a subregion that evades the bound constraints of the entire search region (as indicated by the dashed lines). In such an event, the subregion is projected back into the feasible parameter space along the directions of those parameters for which the bound constraints of the entire search region are violated.

There are two further possibilities for the size specification of a subsequent subregion. These arise when one or more of the active subregion parameter bound constraints are coincident with those parameter bound constraints of the entire search region (as for the optimal points of subregions 3 and 4). Firstly, if some of the remaining subregion bound constraints of the previous optimal point are active (as for the optimal point of subregion 3), then the size of the subregion is reduced only in those parameters that are constrained to the bounds of the entire search region, as for subregion 4. Alternatively, if all of the remaining subregion bound constraints of the previous optimal point are inactive (as for the optimal point of subregion 4), then the optimal point is again regarded as an approximation to the true optimal point, and the entire subregion is reduced, as for subregion 5, to enable convergence to an optimal point that lies on the boundary of the entire search region.

Finally, to avoid the range of the observed response values becoming too small relative to the range of the noise, and thereby corrupting the fitted response surface, a minimum range is specified for each parameter beyond which no further reductions are permitted. This iterative process continues until it either converges to an optimal point or a maximum number of permitted response surface constructions have been performed.

Combined Design Approach

The components of the design approach used in this paper are the PDE method of surface parameterization; the panel method PMARC for subsonic analysis; the central composite experimental design and RSM; the BFGS quasi Newton method of optimization; and, finally, the sequential penalty function and active set methods of constraint satisfaction.

The first of these components, the PDE method, is used to describe the geometry of a baseline flying wing in terms of a number of parameters. Four of these parameters are chosen to be varied in the design process, whereas the remaining are fixed. The baseline wing is then considered to be the center point of a central composite design that spans some chosen subregion of the flying wing's design space. The coefficients of lift of this baseline flying wing and those flying wings corresponding to the cube and star points of the central composite design are then estimated using PMARC. A second-order response surface is fitted to this lift data, which is then optimized globally using the BFGS quasi Newton method (and a number of alternative starting points) subject to the wing's plan area constraint and the parameter bound constraints of the subregion of the design space. During this optimization, the plan area constraint is satisfied using the sequential penalty function method, whereas the parameter bound constraints are satisfied using the active set method. Each of the optimal points of this response surface is then used to select smaller subregions as starting points for the strategy described in the preceding section.

Results

To recap, the wing design parameters that are allowed to vary in the optimization process are the sweep parameter x_t, the derivative boundary condition parameters s_r and s_t, and, finally, the smoothing parameter a. The first problem considered is the design of a wing that is uncambered and untwisted (i.e., with $c = 0$ and $\alpha = 0$ deg). (The remaining fixed parameters are given the same values as for the baseline flying wing.) To generate lift, the wing is set to an angle of attack of 5 deg.

An initial response surface is used to approximate the coefficient of lift over a large region of the design space. The RMS of this initial response surface is 8.156×10^{-5}, whereas the total variation of the coefficient of lift data obtained using the central composite design is 0.2732. The small value of the RMS compared to the total variation of the coefficient of lift indicates that a reasonable

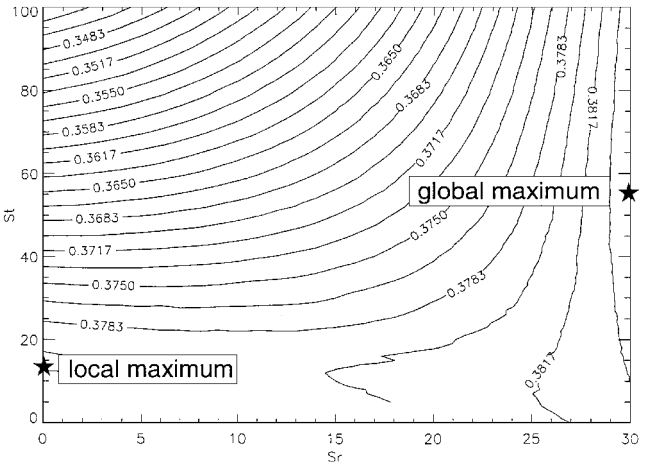

Fig. 5 Contour plot of the variation of the coefficient of lift with s_r and s_t, where x_t = 0.0 and the plan area constraint is satisfied by the elimination of a.

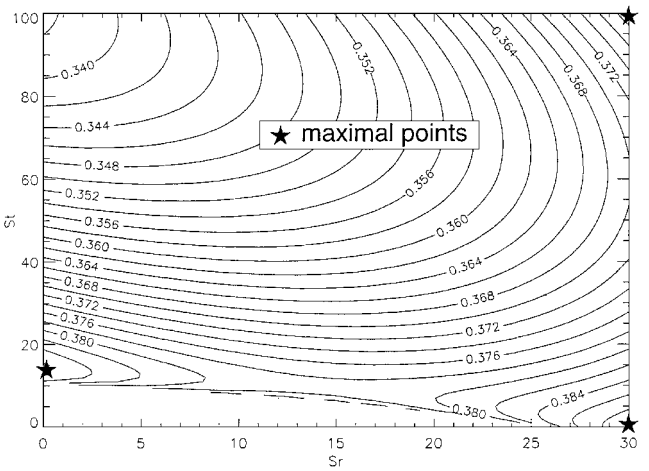

Fig. 6 Contour plot of the variation of the response surface with s_r and s_t, where x_t = 0 and the plan area constraint is satisfied by the elimination of a.

approximation of the coefficient of lift data has been obtained using the second-order regression equation. The quality of this response surface approximation can also be judged by comparing Fig. 5, which illustrates the variation of the coefficient of lift with respect to the design parameters s_r and s_t (where the sweep parameter x_t has been set to zero and the plan area constraint is satisfied by the elimination of the smoothing parameter a), with Fig. 6, which illustrates the variation of the response surface over the same domain of feasible parameter space. (Figure 5 shows the jagged contour lines in the regions where the variation of the lift is small and, also, the troublesome plateau region surrounding the saddle point in the lower left-hand quadrant.) Although, over such a large region, the response surface cannot be expected to exhibit the same variation as the coefficient of lift, some of the local features are actually represented remarkably well. In particular, the local maximum in the lower left-hand corner of these two figures has been identified almost exactly.

The optimization of the initial response surface yields three optimal points, which, apart from the value of x_t, correspond to the local maximum in the lower left-hand corner and those in the upper and lower right-hand corners of Fig. 6. The sequential response surface optimization, initiated from the optimal point in the lower left-hand corner, converges to the nearby true locally maximal solution. However, it can be seen from Fig. 5 that this is not the globally maximal point which is sought. The sequential response surface optimizations initiated from the other two optimal points yield approximately the same final design, which, again apart from the value of x_t, correspond to the true global maximum of Fig. 5. The best of these two final designs has the following parameter values:

$$x_t = 1.502 \qquad s_r = 30.0 \qquad s_t = 58.604 \qquad a = 5.482$$

and has similar response surface and coefficient of lift values, which, when rounded off to four decimal places, are both equal to 0.3865.

Figure 7 illustrates this final untwisted flying-wing design. A principal and perhaps surprising feature of this final design is its flared wing tips. However, these flared wing tips do bear some similarity to wing tip endplates or the more sophisticated winglet.[21] The physical mechanism by which a wing generates lift is the existence of a higher pressure on its lower surface and a lower pressure on its upper surface. At the wing tips this net pressure imbalance forces the air to flow around the tips from the higher pressure region below to the lower pressure region above and thereby reduces the lift near the tip. This tendency for the flow to leak around the wing tips also creates a swirling motion that trails behind the wing tips, i.e., a wing-tip vortex. These wing-tip vortices result in a lift dependent component of drag, known as induced drag, and, more relevant to the present design criterion, a further reduction in the lift of the wing. Endplates are vertical plates that are mounted at the tips of the wing and prevent the air from curling around the tips. This increases the effective span of the wing, allowing significant lift to extend further toward the wing tips and also reduces the induced drag. Winglets are a far more advanced version of the simple endplate that are twisted and cambered in order to create a forward component of lift, which acts as a negative drag.

To reduce computational expense, the wakes used in the present implementation of PMARC were prescribed rather than being allowed to develop to a converged solution. Therefore, the trailing wing-tip vortices are not modeled with sufficient accuracy to predict the effects that changes in the shape of the wing tip have upon them. Nevertheless, it is reasonable to postulate that the presence of the flared wing tips would provide a greater barrier to the flow around the tip than would be provided by, for example, a rounded tip.

Figure 8 illustrates the spanwise variation of the coefficient of lift of both this final untwisted and the baseline flying-wing designs. The section coefficient of lift actually increases in the spanwise direction. This is achieved by the aft sweep of the wings, which

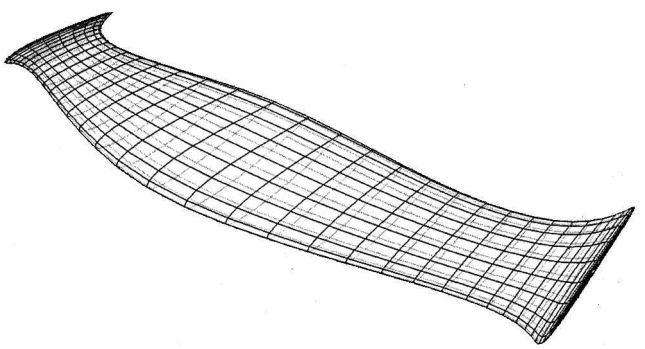

Fig. 7 Best final design of the untwisted flying-wing design problem.

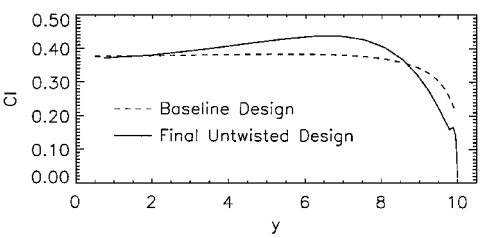

Fig. 8 Spanwise variation of the section coefficients of lift of the best final design of the untwisted flying-wing design problem.

diverts the flow outboard. It appears, therefore, that the flared wing tips create a sheltered region where this diverted flow is harnessed and able to create greater section coefficients of lift.

To investigate the effect that alternative aerofoil boundary conditions will have on the design of a flying wing, the camber c of the root aerofoil boundary condition is set to 0.02. With these modified boundary conditions the initial response surface has a RMS of 4.444×10^{-4}, and the total variation of the lift values obtained using the central composite design is 4.559. These values again indicate a reasonable fit of the second-order polynomial to the coefficient of lift data. The optimization of this initial response surface yields two optimal points from which to initiate the sequential response surface optimizations. The optimizations from these two optimal points converge to approximately the same final wing designs; the best of which has the following parameter values:

$$x_t = 1.686 \qquad s_r = 25.154 \qquad s_t = 0.000 \qquad a = 1.000$$

and response surface and coefficient of lift values of 0.6602 and 0.6585, respectively. In contrast to the preceding wing design problem, where both s_t and a attained relatively large values, in the present problem they have both reached their minimum permitted values. This is not surprising. Because the cambered root aerofoil now generates more lift than the symmetric tip aerofoil, the tip boundary conditions naturally reduce in magnitude and therefore allow the root boundary conditions to propagate further along the span of the wing. This final wing design, which is illustrated in Fig. 9, appears more conventional than the earlier untwisted flying-wing design.

The design problem is now extended further by setting the value of α at the wing-tip boundary condition to be -5 deg such that the wing has washout. The RMS of the initial response surface approximation is 7.217×10^{-4}, and the total range of the coefficient of lift values obtained using the central composite design is 0.5537. As for the cambered wing design problem, two optimal points were obtained from the optimization of this initial response surface, which both subsequently converged to similar final flying-wing designs. Not surprisingly, these final twisted wing designs are similar to those obtained in the cambered flying-wing design problem. The best final twisted flying wing, which is illustrated in Fig. 10, has the following parameter values:

$$x_t = 2.196 \qquad s_r = 25.513 \qquad s_t = 0.000 \qquad a = 1.000$$

and response surface and coefficient of lift values of 0.6308 and 0.6432, respectively. The value of the sweep parameter x_t is appreciably greater for this design than for the cambered flying-wing design. Figure 11 illustrates the spanwise variation of the section coefficients of lift of the final cambered and final twisted flying-wing designs. In both the cambered and twisted final wing designs, the sweep back of the wings diverts the flow outboard and enables significant lift to propagate further along the span.

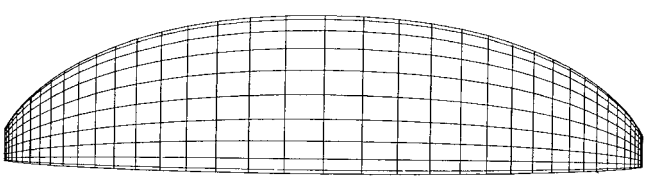

Fig. 9 Best final design of the cambered flying-wing design problem.

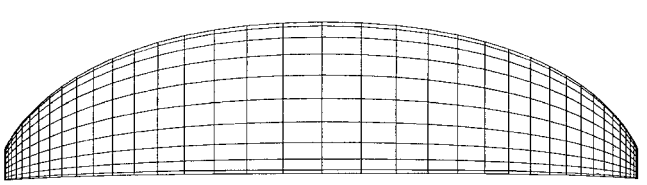

Fig. 10 Best final design of the twisted flying-wing design problem.

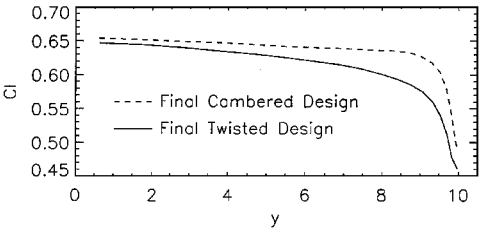

Fig. 11 Spanwise variation of the section coefficients of lift of the best final designs of the cambered and twisted flying-wing design problems.

Conclusions

An approach for optimal aerodynamic design, which is both efficient and robust, has been illustrated. This approach implements two innovative approaches to aerodynamic design, namely the PDE method and RSM. The PDE method's ability to parameterize complex surfaces in terms of a small number of shape parameters enables the computational expense of numerical optimization to be dramatically reduced, whereas the implementation of techniques from RSM combats the inefficacy stemming from noisy lift data.

This design approach was applied successfully to three flying-wing design problems in each of which the aim is to maximize the wing's subsonic lift while maintaining a fixed plan area. The first of these was the design of an untwisted wing with symmetric root and tip aerofoils. An interesting final untwisted flying-wing design was obtained that had endplate-like buffers at its tips. This flying-wing design illustrates that there is sufficient scope in the surface parameterization for a wide range of shapes. More conventional wings were obtained when root camber and washout were introduced. The absence of the wing-tip buffers in these two design problems arises because the root aerofoils generate more lift than the tip aerofoils and result, therefore, in a reduction of the wing-tip derivative boundary conditions.

Acknowledgment

The authors gratefully acknowledge financial support (awarded as a research studentship and, also, as Research Grant GR/L11366) from the Engineering and Physical Sciences Research Council.

References

[1] Northrop, J. K., "The Development of All-Wing Aircraft: 35th Wilbur Wright Memorial Lecture," *The Journal of the Royal Aeronautical Society*, Vol. 51, 1947, pp. 481–510.

[2] Sears, W. R., "Flying Wing Could Stealthily Reappear," *Aerospace America*, Vol. 37, July 1987, pp. 16–19.

[3] Biddle, W., "Skeleton Alleged in the Stealth Bomber's Closet," *Science*, Vol. 244, May 1989, pp. 650, 651.

[4] Labrujère, Th. E., and Slooff, J. W., "Computational Methods for the Aerodynamic Design of Aircraft Components," *Annual Review of Fluid Mechanics*, Vol. 25, 1993, pp. 183–214.

[5] Hicks, R. M., and Henne, P. A., "Wing Design by Numerical Optimization," AIAA Paper 77-1247, Aug. 1977.

[6] Aidala, P. V., Davis, W. H., Jr., and Mason, W. H., "Smart Aerodynamic Optimization," AIAA Paper 83-1863, 1983.

[7] Hutchison, M., Unger, E., Mason, W., Grossman, B., and Haftka, R., "Variable-Complexity Aerodynamic Optimization of an HSCT Wing Using Structural Wing-Weight Equations," AIAA Paper 92-0212, Jan. 1992.

[8] Bloor, M. I. G., and Wilson, M. J., "Using Partial Differential Equations to Generate Free-Form Surfaces," *Computer-Aided Design*, Vol. 22, No. 4, 1990, pp. 202–212.

[9] Bloor, M. I. G., and Wilson, M. J., "Efficient Parameterization of Generic Aircraft Geometry," *Journal of Aircraft*, Vol. 32, No. 6, 1995, pp. 1269–1275.

[10] Smith, R. E., Bloor, M. I. G., Wilson, M. J., and Thomas, A. M., "Rapid Airplane Parametric Input Design (RAPID)," AIAA Paper 95-1687, June 1995.

[11] Sevant, N. E., Bloor, M. I. G., and Wilson, M. J., "Aerodynamic Design of a Wing-Body Combination," *Creating Fair and Shape-Preserving Curves and Surfaces*, edited by H. Nowacki, P. D. Kaklis, and B. G. Teubner,

Stuttgart/Leipzig, Germany, 1998, pp. 271–280.

[12]Dekanski, C. W., Bloor, M. I. G., and Wilson, M. J., "The Generation of Propeller Blade Geometries Using the PDE Method," *Journal of Ship Research*, Vol. 39, No. 2, 1995, pp. 108–116.

[13]Bloor, M. I. G., and Wilson, M. J., "Spectral Approximations to PDE Surfaces," *Computer-Aided Design*, Vol. 28, No. 2, 1996, pp. 145–152.

[14]Ashby, D. L., Dudley, M. R., Iguchi, S. K., Browne, L., and Katz, J., "Potential Flow Theory and Operation Guide for the Panel Code PMARC," NASA TM 102851, 1991.

[15]Katz, J., and Plotkin, A., *Low-Speed Aerodynamics: From Wing Theory to Panel Methods*, McGraw–Hill, New York, 1991, pp. 237–412.

[16]Press, W. H., Teukolsky, S. A., Vetterling, W. T., and Flannery, B. P., *Numerical Recipes in FORTRAN*, Cambridge Univ. Press, Cambridge, England, U.K., 1992, pp. 374–379.

[17]Fletcher, R., *Practical Methods of Optimization*, Wiley, New York, 1987.

[18]Montgomery, D. C., *Design and Analysis of Experiments*, Wiley, New York, 1991.

[19]Toropov, V. V., "Simulation Approach to Structural Optimization," *Structural Optimization*, Vol. 1, No. 1, 1989, pp. 37–46.

[20]Narducci, R., Grossman, B., Valorani, M., Dadone, A., and Haftka, R. T., "Optimization Methods for Non-Smooth or Noisy Objective Functions in Fluid Design Problems," AIAA Paper 95-1648, June 1995.

[21]Raymer, D. P., *Aircraft Design: A Conceptual Approach*, AIAA, Washington, DC, 1992, p. 64.